PAPER

Raman spectra of twisted bilayer graphene close to the magic angle

To cite this article: Tiago C Barbosa *et al* 2022 *2D Mater.* **9** 025007

2D Materials

PAPER

Raman spectra of twisted bilayer graphene close to the magic angle

Tiago C Barbosa[1,2,8], Andreij C Gadelha[1,3,8], Douglas A A Ohlberg[4], Kenji Watanabe[5], Takashi Taniguchi[6], Gilberto Medeiros-Ribeiro[7], Ado Jorio[1,9] and Leonardo C Campos[1,2,9,*]

[1] Physics Department, Universidade Federal de Minas Gerais, Belo Horizonte, MG 31270-901, Brazil
[2] Center of Technology in Nanomaterials and Graphene, Universidade Federal de Minas Gerais, Technological Park of Belo Horizonte, Belo Horizonte, MG 31270-901, Brazil
[3] Department of Physics and JILA, University of Colorado at Boulder, Boulder, CO, 80309, United States of America
[4] Microscopy Center, Universidade Federal de Minas Gerais, Belo Horizonte, MG 31270-901, Brazil
[5] Research Center for Functional Materials, National Institute for Materials Science (NIMS), 1-1 Namiki, Tsukuba 305-0044, Japan
[6] International Center for Materials Nanoarchitectonics, National Institute for Materials Science (NIMS), 1-1 Namiki, Tsukuba 305-0044, Japan
[7] Computer Science Department, Universidade Federal de Minas Gerais, Belo Horizonte, MG 31270-901, Brazil
[8] These authors contributed equally to this work.
[9] These authors equally supervised the project.
[*] Author to whom any correspondence should be addressed.

E-mail: lccampos@fisica.ufmg.br

RECEIVED
8 November 2021

REVISED
28 December 2021

ACCEPTED FOR PUBLICATION
13 January 2022

PUBLISHED
1 February 2022

Keywords: Raman spectroscopy, twisted bilayer graphene, magic angle

Supplementary material for this article is available online

Abstract

In this work, we study the Raman spectra of twisted bilayer graphene samples as a function of their twist-angles (θ), ranging from 0.03° to 3.40°, where local θ are determined by analysis of their associated moiré superlattices, as imaged by scanning microwave impedance microscopy. Three standard excitation laser lines are used (457, 532, and 633 nm wavelengths), and the main Raman active graphene bands (G and 2D) are considered. Our results reveal that electron–phonon interaction influences the G band's linewidth close to the magic angle regardless of laser excitation wavelength. Also, the 2D band lineshape in the $\theta < 1°$ regime is dictated by crystal lattice and depends on both the Bernal (AB and BA) stacking bilayer graphene and strain soliton regions (SP) (Gadelha *et al* 2021 *Nature* **590** 405–9). We propose a geometrical model to explain the 2D lineshape variations, and from it, we estimate the SP width when moving towards the magic angle.

1. Introduction

Van der Walls heterostructures (vdW-H) are formed by assembling different 2D materials, and they may present distinct electrical, optical, and mechanical properties from their counterparts [1–3]. The study of vdW-H revealed that the properties of the final structure depend on the chosen materials and, in the case of twisted bilayer or few-layer materials, the relative twisting angle (θ) between each atomic layer plays an important role [4]. In 2018, researchers showed that twisted bilayer graphene (TBG) devices with relative twist angles close to 1.1°, known as the magic angle (θ_M) [5, 6], behave as strongly interacting systems that allow unconventional superconductivity [7]. Such TBG devices present phase transitions from correlated insulators, conductors, superconductors, and even ferromagnetic phases [8–13]. This unique system also presents interesting electron-phonon related phenomena [14, 15], which may shed light into the role of this interaction in the aforementioned phase transitions [16–19].

Raman spectroscopy has been widely used to study graphene devices due to its several advantages: it is a fast and non-destructive technique that allows investigation of strain, doping, disorder, electron-phonon interaction, and many other aspects of such devices [20–23]. Raman spectra of what we call here large-angle TBG devices, which means θ ranging from 3° to 30°, has been largely studied [24–35] and a review on the topic can be found in [14]. The most important aspect in this large angle range is a plethora

of new peaks originated from the moiré superlattice and an increase in the main G and 2D peaks intensity in certain twist angles, which in turn provides a simple way of accurately determining the TBG twist angle [32, 34]. More recently, nano-Raman measurements revealed that TBG with angles smaller than θ_M undergo a self-organized crystal lattice reconstruction [36]. In this range of twist angles, TBG show periodical triangular areas of alternating Bernal (AB and BA) stacking domains, separated by shear soliton regions (SP), with AA-stacked regions at the vertices of the triangular areas [36].

This work presents micro-Raman study of TBG samples in the twist-angle range around the magic angle, i.e. for θ ranging from 0.03° to 3.40°. We investigated the Raman spectra of TBG devices with three different excitation lasers, and we show that samples with angles close to 0° have their Raman spectra dominated by Bernal stacking bilayer graphene. Our data also reveal an increasing contribution of AA-stacking and soliton regions to the behavior of the sample with increasing angle towards the magic angle, as proposed theoretically in band structure calculations by Nguyen *et al* [37]. Furthermore, we analyzed qualitatively electron-phonon interactions in TBG devices in terms of the Kohn anomaly process, and we related the increase in the Raman G band full width at half maximum close to the magic angle with the appearance of a flat band in the band structure of such systems [5, 6, 38].

2. Methods

The graphene samples were obtained by the standard scotch tape method [39] and deposited over Si substrate covered by 285 nm thick thermally oxidized silicon. The TBG samples were fabricated through a tear-and-stack method [40] with the aid of a polydimethylsiloxene (PDMS) pyramid stamp (PS) reported elsewhere [36, 41]. Described briefly, a polycarbonate membrane is attached to a PS, aligned over a region of the Si substrate containing the graphene flake, and pressed into contact with it while raising the sample temperature. A few minutes later, the sample is allowed to cool down, and the stamp is retracted from the substrate, causing the portion of flake adhering to the stamp to tear loose from the rest of the flake that remains on the substrate. After that, the substrate with the remaining graphene sheet is rotated to the desired twist angle relative to the fixed stamp orientation, and the whole process with the PS is repeated to pick up the rest of flake off the substrate. At last, the TBG is attached to the stamp and can be deposited over any chosen substrate. Additionally, we have picked up a hexagonal boron nitride (hBN) flake as a supporting substrate for the TBG, an atomically flat surface free of dangling bonds or charge traps [42]. In the end, we deposited our heterostructure over a microscope glass slide, as depicted in figure 1(a). The fabricated TBG samples were then characterized by scanning microwave impedance microscopy (sMIM). The sMIM is a near-field technique that uses a microwave source coupled to an atomic force microscope (AFM) probe. As the tip scans the sample, local variations in permittivity and conductivity can be analyzed and translated in terms of sample's capacitance and resistance variations. Recently, sMIM has proved to be a very powerful tool to study TBG superlattices with ∼1 nm spatial resolution, and the obtained results allow the observation of the moiré patterns of the probed samples [43]. Therefore, the sMIM images reveal different moiré patterns for different twist angles as shown in figure 1 for (b) $\theta = 0.17°$, (c) 1.20°, and (d) 3.40°. Each twist angle was estimated by the expression $\theta = 2.\arcsin(a_G/2.L_M)$ [44], where $a_G = 0.246$ nm is the graphene crystal lattice constant and L_M is the θ-dependent moiré superlattice periodicity, obtained from the sMIM images.

Thereafter, we acquired hyperspectral Raman maps of the TBG using a WITec Alpha300R system, with 1.0 mW laser power at the sample, focused by a 100× objective with NA = 0.9. Finally, hyperspectral Raman maps and sMIM images are combined, enabling identification of homogeneous moiré patterns from which the Raman data were acquired. In each homogeneous moiré pattern region, Raman spectra are acquired from different points and averaged to obtain the corresponding representative spectrum, as shown in figure S4 (available online at stacks.iop.org/2DM/9/025007/mmedia) from the supporting information. Through the rest of this work, all the analyses were carried out on the average spectrum obtained from each of these homogeneous regions. For further details on the Raman maps and sMIM images combination, please refer to the supporting information. This process was performed using three different excitation laser wavelengths, namely 457 nm, 532 nm and 633 nm.

3. General trends of the Raman spectrum

The first comparison between Raman spectra of Bernal stacking bilayer graphene and TBG with different twist angles is depicted in figure 1(e), measured with a 532 nm excitation laser wavelength. We focus our attention on the most prominent graphene Raman peaks: the G band around 1580 cm^{-1}, which is a first-order Raman peak associated with the doubly degenerate (iTO and LO) phonon mode at the Brillouin zone center, and the 2D band around 2700 cm^{-1}, which is a dispersive second-order Raman peak involving two iTO phonons near the K point at the edges of the Brillouin zone [21, 45, 46]. At first glance, the major difference in the G band with respect to θ is an increase in its linewidth (Γ_G) at the angle close to the magic angle (see $\theta = 1.20°$ in figure 1(e)) [36]. Regarding the 2D band, note

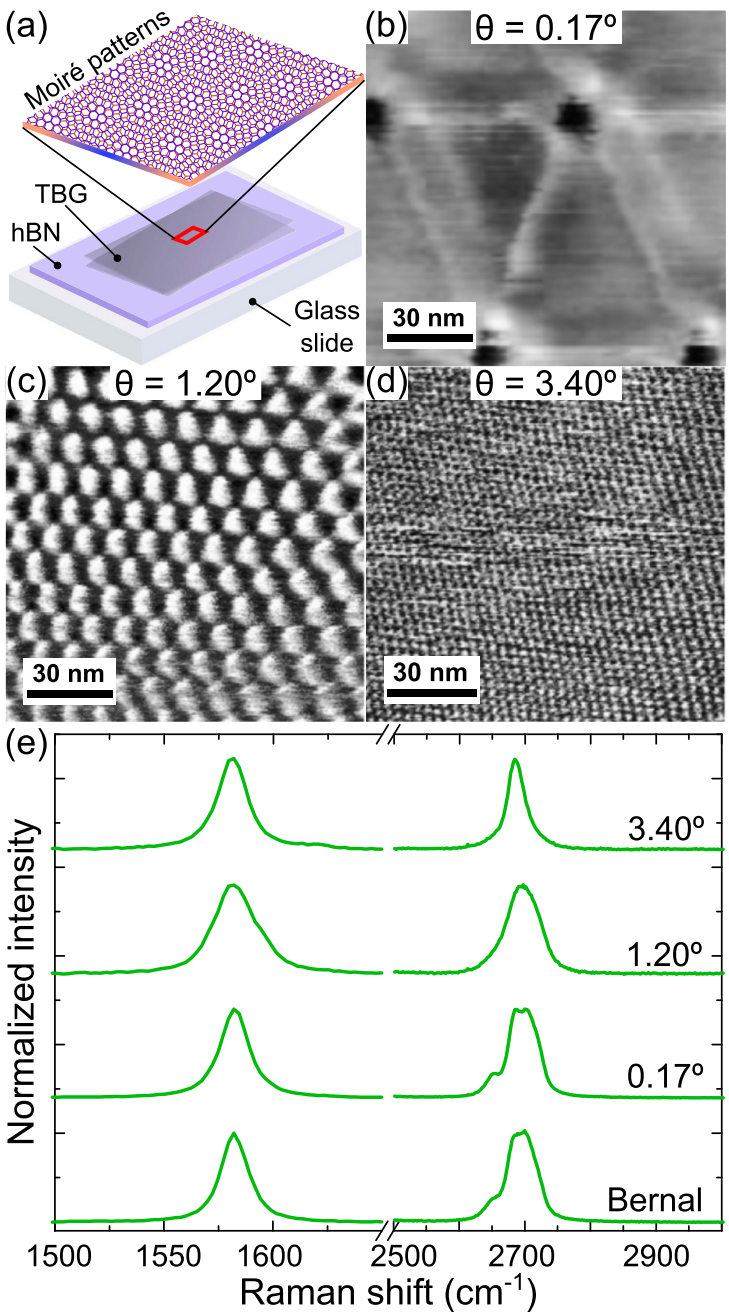

Figure 1. (a) Schematics of our hBN-TBG sample produced through a tear-and-stack method with the aid of a PDMS pyramid stamp deposited over a glass slide—inset shows a schematic of a moiré pattern that can be found in TBG samples. Superlattices for samples with (b) $\theta = 0.17°$, (c) 1.20°, and (d) 3.40° twist angles, measured by sMIM. (e) G and 2D band Raman spectra of a Bernal bilayer graphene and the samples shown in (b)–(d) (see labels near each spectrum), acquired with a 532 nm excitation laser.

that the $\theta = 0.17°$ spectra resemble the bilayer graphene Bernal stacking spectrum [45], whereas the spectra for $\theta = 1.20°$ and 3.40° reveal different shapes.

To further investigate the Raman spectra dependence on the TBG twist angle, several samples ranging from 0.03° to 3.40° were measured with different excitation laser wavelengths, as shown in figure 2 for (a) 457 nm, (b) 532 nm, and (c) 633 nm—the data are normalized with respect to each G and 2D bands spectra for clarity. The G band of each spectrum is fitted with a single Lorentzian peak and analyzed in terms of its frequency (ω_G) and full width at half maximum (Γ_G). There is no clear dependence of ω_G on the twist angle, as highlighted in figure 3(a). On the other hand, there seems to be a peak broadening for samples with θ close to θ_M. Additional AFM topography analyses were also performed, revealing a roughness in the order of 1 Angstrom (figure S2), and the absence of wrinkles or corrugations. The Γ_G dependence on the twist angle will be further discussed in more detail in session 5.

The 2D band of each spectrum is evaluated in terms of its line shape and of a medium frequency ($\tilde{\omega_{2D}}$), which was defined as $\tilde{\omega_{2D}} = \int (I(\omega).\omega)d\omega / \int I(\omega).d\omega$, where $I(\omega)$ is the

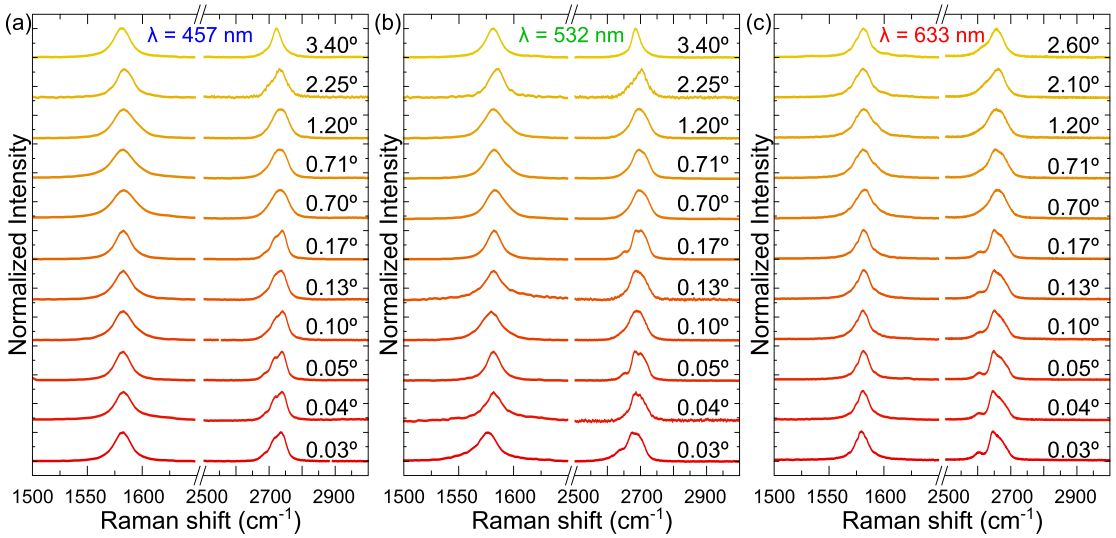

Figure 2. Raman spectra of TBG with twist angles ranging from 0.03° to 3.40° (see labels near each spectrum), measured with (a) 457 nm, (b) 532 nm, and (c) 633 nm excitation lasers wavelengths.

Raman spectrum intensity, ω is its frequency, and the integrals were evaluated in the 2D band region (2600 $cm^{-1} < \omega <$3000 cm^{-1} range). Yet again, there is no clear dependence of $\omega_{2D}^{\sim}$ on θ, while preserving the expected dispersive behavior with respect to the energy of the incident laser (figure 3(b)) [21, 45]. Note that the 2D band line shape of samples with twist angles close to 0° resembles bilayer graphene with Bernal stacking, see figure 2, which can be described in terms of four Lorentzian peaks [21, 45]. In figure 2, we can also see that the 2D band line shape gradually changes and become more and more similar to AA stacking or SP soliton regions (figure 3(b) in [36]) with increasing θ towards the magic angle, which can be more apparent for $\theta \geqslant$0.70°. This tendency is related to a more significant contribution from AA stacking or soliton regions to the measured Raman spectra in samples with $\theta \geqslant$0.70°, as noted by Nguyen *et al* [37], which will be discussed in more detail in the next section.

The use of Raman spectroscopy to evaluate mechanical strain and charge doping in graphene was introduced by Lee *et al* [47]. The correlation between the medium 2D band and G band frequencies (figure 3(c)) reveals that the data spread mainly at a 2.2 slope, indicating that our samples present different mechanical strain and no doping differences among samples [47]. Despite revealing different mechanical strain, there is no clear dependence of strain on θ.

4. The 2D band line shape

The 2D band (also called G′ in the literature) is the result of a combination of allowed double-resonant two-phonon Raman scattering processes, with the lineshape depending on the specific electronic and phononic structure of the material, differing for different types of sp^2 carbons [45, 48–53], as well as on the twist-angle in the large-angle regime [28]. As mentioned before, in the angle regime studied here, there is a gradual change in the 2D band line shape with increasing twist angle, which can be noticed in figure 2 for all laser lines. Local nano-Raman measurements (or tip enhanced Raman spectroscopy—TERS) can directly probe the AB/BA and the AA/SP regions, revealing different 2D band spectra, as already shown by Gadelha *et al* [36]. In this sense, the micro-Raman 2D band spectra have contributions from both regions. So, starting from $\theta = 0$, each spectrum can be fitted with a combination of a Bernal (AB and BA) 2D band spectrum (S_{AB}) and a free pseudo-Voigt function (S_{pV}) [54]. S_{AB} is a four-peaks structure which depends on the excitation laser line [45, 55]. S_{pV} is a generic function that varies from a Lorentzian to a Gaussian distribution [56, 57], used here as a practical approximation to address the emission from the AA/SP regions, which are present in the reconstructed TBG (rTBG) in low twist angles [36]. Therefore, the total spectrum (S_T) is a combination of these two features ($S_T = \alpha S_{AB} + \beta S_{pV}$), with α and β measuring the relative contribution from S_{AB} and S_{pV}, respectively, i.e. ($\alpha \to 1$, $\beta \to 0$) for $\theta \to 0$ and ($\alpha \to 0$, $\beta \to 1$) in the large-angle limit. Indeed, at twist angles larger than θ_M, the S_{pV} function alone fits the 2D bands considerably well. To obtain more insights on the proposed model, TERS measurements were performed on our rTBG samples, and the spectra from the AB/BA and AA/SP regions were obtained (figure S5). The proposed fitting model was applied to these spectra, and we note that the AB/BA spectrum is best described by the Bernal spectrum ($\alpha \to 1$, $\beta \to 0$) (figure S5(a)) as well as the AA/SP spectrum is best described by the pseudo-Voigt function ($\alpha \to 0$,

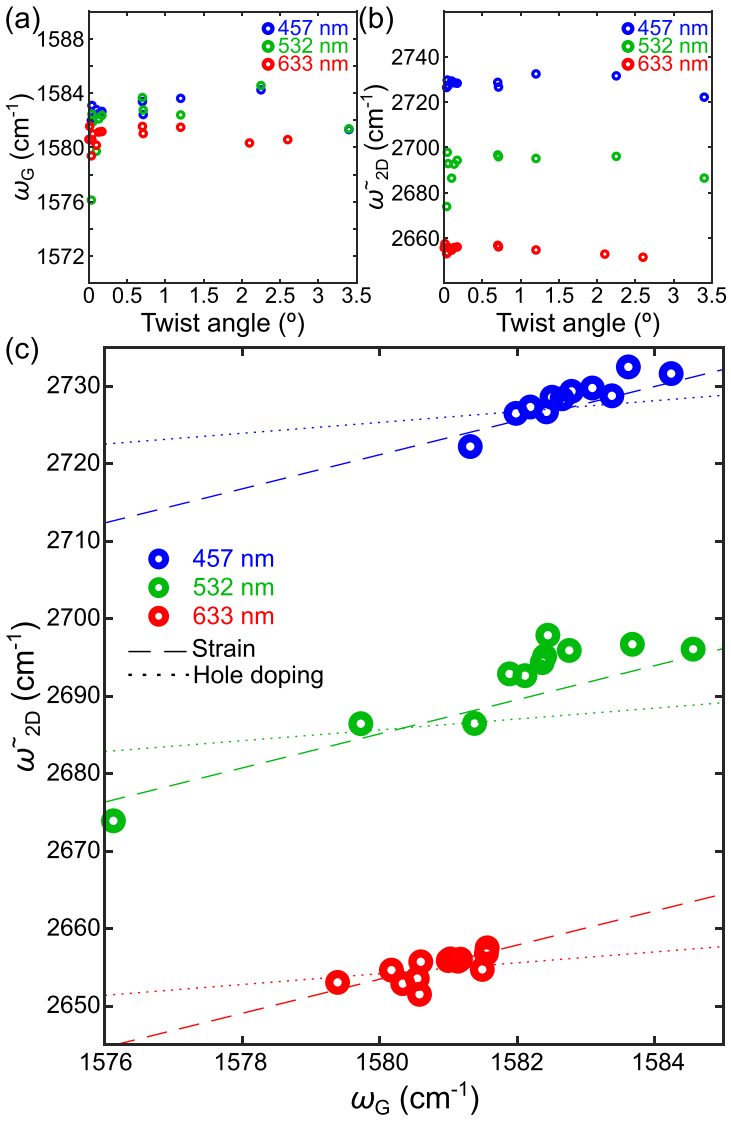

Figure 3. Raman shift of (a) G band, and (b) medium 2D band. (c) Medium 2D band Raman shift ($\tilde{\omega_{2D}}$) and G band Raman shift (ω_G) relation—the dashed (dotted) lines with 2.2 (0.7) slope reveal the strain (doping) tendencies [47], rigidly shifted to match the data for each excitation laser.

$\beta \to 1$) (figure S5(b)), which further supports the proposed analysis. More details on the TERS measurements and setup can be found in section 5 of the supporting information.

The θ-dependent 2D spectral change is explained as follows: at angles close to 0° (figure 4(a)), the spectrum is dominated by Bernal regions, and the contribution of the pseudo-Voigt function is insignificant ($\alpha \approx 1$, $\beta \approx 0$). Closer to the middle range between 0° and the magic angle (figure 4(b)), we see an increase in the contribution of the pseudo-Voigt function, indicating a more considerable contribution from AA/SP regions to the overall spectrum. Closer to the magic angle (figure 4(c)), the contribution of the pseudo-Voigt function is stronger than Bernal's one indicating a dominance of the AA/SP region or from the large-angle TBG spectra. Finally, at twist angles larger than θ_M (figure 4(d)), insignificant contribution from the Bernal spectrum is observed, and the pseudo-Voigt function entirely dominates ($\alpha \approx 0$, $\beta \approx 1$), as expected, since the Bernal stacking ceases to exist above θ_M [58].

In order to relate this general trend of the 2D band spectra with the TBG lattice, a geometric model based on the size of the AB/BA and AA/SP regions was used. The contribution of each component to the overall spectrum area was analyzed, and related to the α and β spectral contributions. Then, these parameters can be related with their geometric counterpart in the TBG lattice, which were called A_{AB} for the Bernal area, and A_{SP} for the AA/SP area (inset in figure 4(e)). At last, the α/β ratio is given by the A_{AB}/A_{SP} ratio, and can be expressed in terms of the soliton width (W_{SP}), the TBG twist angle (θ) and the graphene crystal lattice constant (a_G):

$$\frac{\alpha}{\beta} = \frac{A_{AB}}{A_{SP}} = \frac{\frac{a_G}{4.\sin\frac{\theta}{2}} - W_{SP}.\sqrt{3} + \frac{3.{W_{SP}}^2.\sin\frac{\theta}{2}}{a_G}}{W_{SP}.\sqrt{3} - \frac{3.{W_{SP}}^2.\sin\frac{\theta}{2}}{a_G}}. \quad (1)$$

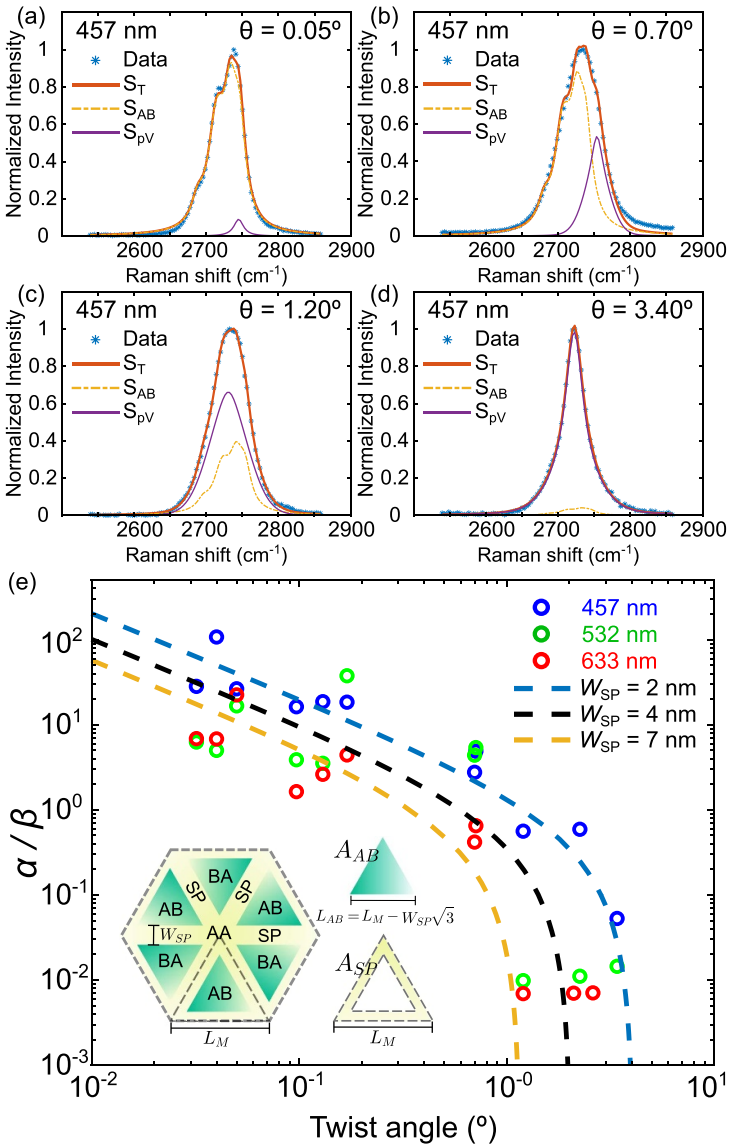

Figure 4. 2D band spectra for samples with θ equals to (a) 0.05°, (b) 0.70°, (c) 1.20° and (d) 3.40°, measured with a 457 nm laser wavelength and fitted with a combination of a Bernal stacking spectrum, S_{AB}, and a pseudo-Voigt function, S_{pV}. The α and β fitting parameters were left free to vary, without any bonding condition; (e) α/β ratio as a function of twist angle in a log-log scale for all laser lines, with the data points coming from the spectral analysis, and the black dashed-line representing the data points fitted with the geometric model summarized in the inset (see text for details) for $W_{SP} = 4$ nm—curves for $W_{SP} = 2$ nm (blue dashed-line) and 7 nm (orange dashed-line) were also plotted for comparison.

Therefore, the above expression was used to fit the α/β ratio as a function of the twist angle, with W_{SP} as a free adjusting parameter, as shown in figure 4(e) in a log-log scale for all laser lines. After the analysis of the data with the proposed geometric model, the obtained soliton width was approximately $W_{SP} = (4 \pm 3)$ nm, which agrees quite well with theory [59] and measurements performed through different experimental techniques [60, 61]. In figure 4(e) we exhibit the best fitted α/β curve with $W_{SP} = 4$ nm (dashed black curve), but we also provide $W_{SP} = 2$ nm (blue) and $W_{SP} = 7$ nm (orange) curves for comparison. The tendency observed in figure 4(e) is not laser-dependent, which corroborates the proposed geometric model. At this point, it is important to highlight that our model ignores a possible W_{SP} dependence on the twist angle [59] and, despite being a simple phenomenological model, it describes the phenomenology and our data significantly well, introducing a new approach to address the width of solitons in the reconstruction regime of TBG samples. The W_{SP} value found here should be applicable to the soliton width towards small moiré pattern unit cells, where the soliton width plays a more relevant role for the A_{AB}/A_{SP} ratio.

5. The G band FWHM

Now we turn our attention to the dependence of Γ_G on θ. Previous works reported an increase in Γ_G with decreasing twist angle in the large-angle range below $\theta = 5°$ [27]. Our results reveal a tendency to reach

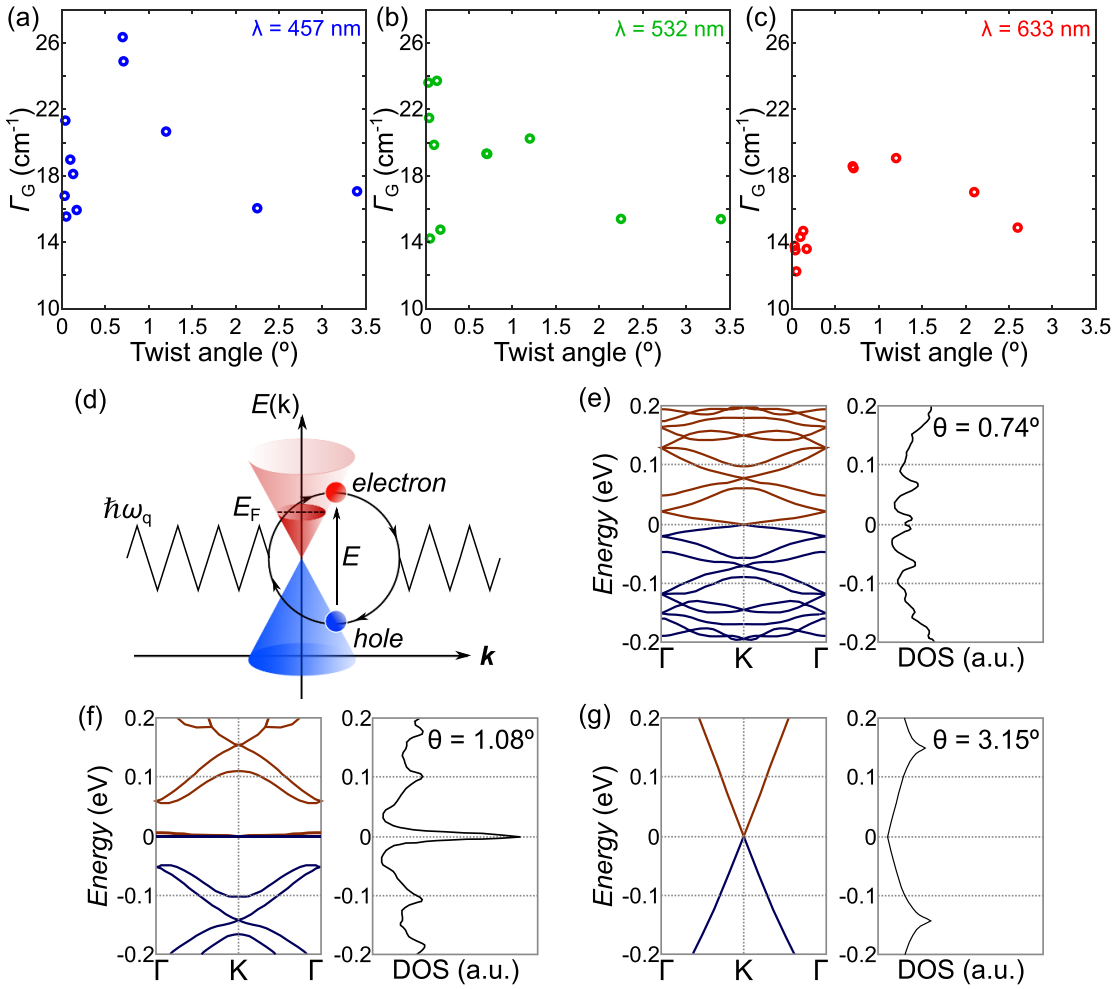

Figure 5. G band full width at half maximum (Γ_G) dependence on the TBG twist angle for (a) 457 nm, (b) 532 nm, and (c) 633 nm (adapted from Gadelha *et al* [36]) excitation laser wavelengths. The data reveal a maxima of Γ_G close to θ_M for all measured laser lines, while the Γ_G spread for $\theta \to 0°$ might be due to sample inhomogeneity; (d) schematics of the electron-phonon interactions in the Kohn anomaly process in graphene (adapted from Hasdeo *et al* [62]); band structure and DOS of TBG samples calculated through a tight-binding approach for (e) $\theta = 0.74°$, (f) $\theta = 1.08°$ (magic angle), and (g) $\theta = 3.15°$ (the later adapted from Nguyen *et al* [66]). The $\theta = 1.08°$ reveals a flat band at zero energy, which is directly related to the spike in the DOS.

a maximum peak width close to the magic angle for all measured laser lines (figures 5(a)–(c) for 457 nm, 532 nm, and 633 nm, respectively). Figure 5(c) was adapted from Gadelha *et al* [36], where a single excitation energy (633 nm) was used.

The electron–phonon interaction process in graphene is known to cause an increase in the G band full width at half maximum [55, 62–65]. In this process, an initial phonon with frequency ω_q excites an electron–hole pair, which recombines emitting a phonon with energy E, as depicted in figure 5(d) [55, 62–65]. The electron–hole pair creation rate and the recombination rate depend on the allowed electronic states involved and the phonon range of energy. So, when the Fermi energy is in the charge neutrality point, there is a large probability of electron–phonon interaction, thus decreasing the phonon lifetime. This process reveals itself as an increase in the G Raman peak width, as stated by the uncertainty principle [55, 62–65]. In TBG, twist angle changes the energy band and electronic density of states. In this sense, in TBG, the electron-phonon interaction turns stronger due to an increase in the electronic density of states (DOS). Figure 5 also presents three major cases: $\theta < \theta_M$, $\theta = \theta_M$ and $\theta > \theta_M$, as for (e) $\theta = 0.74°$, (f) $\theta = 1.08°$ (magic angle), and (g) $\theta = 3.15°$ (adapted from Nguyen *et al* [66]). Despite the complex band structure of the $\theta = 0.74°$ case, it is clear that its DOS remains in the same order of magnitude as the DOS for $\theta = 3.15°$. Nevertheless, the band structure of the $\theta = 1.08°$ reveals a flat band at zero energy, which causes the DOS to escalate. Therefore, it is expected an increase in Γ_G close to the magic angle, regardless of the laser excitation energy, as revealed by figure 5 and Gadelha *et al* [36]. Nonetheless, it is important to highlight that the presented explanation is qualitative. Further experiments and theoretical studies, ideally with doping,

need to be performed to describe the data results quantitatively.

6. Conclusion

In summary, we presented an investigation of the Raman spectra of TBG with twist angles ranging from 0.03° to 3.40°, with three different laser lines, and our analysis focused on the Raman-active G and 2D bands. The spectra reveal two main θ-dependent phenomena: (a) an increase of the G band width (Γ_G) close to the magic angle, which is understood based on electron-phonon interaction. The increase in Γ_G is expected due to the larger density of states of samples close to the magic angle, increasing the electron–phonon interaction and lowering the phonon lifetime; (b) a variation in the 2D band line shape, which indicates a general trend of an increased relative contribution from AA/SP regions as compared to the Bernal (AB/BA) regions to the Raman spectra of samples with increasing θ for twist angles smaller than the magic angle, according to previous TBG theoretical works [37]. The 2D bands were decomposed in two main contributions: a Bernal stacking spectrum and a pseudo-Voigt function related to the AA/SP regions, which further highlights the decrease in the Bernal stacking contribution to the overall spectra with increasing twist angle. We also proposed a geometric model to further analyze this trend, which became an interesting approach to estimate the soliton width towards small moiré pattern unit cells, found here to be in the $W_{SP} = (4 \pm 3)$ nm range. Therefore, our presented results describe the science of the Raman spectroscopy around the magic angle, and it brings up the importance of Raman spectroscopy as a fast and non-destructive technique in the characterization of TBG devices, a powerful tool for identifying the twist angles of such samples. I.e. a proposed protocol to locate effective magic angle in disordered samples [67] is to raster scan the sample looking for regions with the highest G band linewidth and with small Bernal stacking spectrum contribution to the 2D band spectra.

Data availability statement

All data that support the findings of this study are included within the article (and any supplementary files).

Acknowledgments

This work was supported by CNPq, INCT/ Nanomaterials de Carbono, CAPES and FAPEMIG, Brazil. K W and T T acknowledge support from the JSPS KAKENHI (Grant Numbers 19H05790, 20H00354 and 21H05233).

ORCID iDs

Tiago C Barbosa https://orcid.org/0000-0001-6303-4222
Andreij C Gadelha https://orcid.org/0000-0002-6350-7680
Douglas A A Ohlberg https://orcid.org/0000-0003-1634-0264
Kenji Watanabe https://orcid.org/0000-0003-3701-8119
Takashi Taniguchi https://orcid.org/0000-0002-1467-3105
Gilberto Medeiros-Ribeiro https://orcid.org/0000-0001-5309-2488
Ado Jorio https://orcid.org/0000-0002-5978-2735
Leonardo C Campos https://orcid.org/0000-0001-6792-7554

References

[1] Geim A K and Grigorieva I V 2013 Van der Waals heterostructures *Nature* **499** 419–25
[2] He J, Wang C, Zhou B, Zhao Y, Tao L and Zhang H 2020 2D van der Waals heterostructures: processing, optical properties and applications in ultrafast photonics *Mater. Horizons* **7** 2903–21
[3] Ajayan P, Kim P and Banerjee K 2016 Two-dimensional van der Waals materials *Phys. Today* **69** 38–44
[4] Carr S, Massatt D, Fang S, Cazeaux P, Luskin M and Kaxiras E 2017 Twistronics: manipulating the electronic properties of two-dimensional layered structures through their twist angle *Phys. Rev.* B **95** 1–6
[5] Bistritzer R and MacDonald A H 2011 Moire bands in twisted double-layer graphene *Proc. Natl Acad. Sci.* **108** 12233–7
[6] Suárez Morell E, Correa J D, Vargas P, Pacheco M and Barticevic Z 2010 Flat bands in slightly twisted bilayer graphene: tight-binding calculations *Phys. Rev.* B **82** 121407
[7] Cao Y, Fatemi V, Fang S, Watanabe K, Taniguchi T, Kaxiras E and Jarillo-Herrero P 2018 Unconventional superconductivity in magic-angle graphene superlattices *Nature* **556** 43–50
[8] Cao Y *et al* 2018 Correlated insulator behaviour at half-filling in magic-angle graphene superlattices *Nature* **556** 80–84
[9] Sharpe A L, Fox E J, Barnard A W, Finney J, Watanabe K, Taniguchi T, Kastner M A and Goldhaber-Gordon D 2019 Emergent ferromagnetism near three-quarters filling in twisted bilayer graphene *Science* **365** 605–8
[10] Lu X *et al* 2019 Superconductors, orbital magnets and correlated states in magic-angle bilayer graphene *Nature* **574** 653–7
[11] Yankowitz M, Chen S, Polshyn H, Zhang Y, Watanabe K, Taniguchi T, Graf D, Young A F and Dean C R 2019 Tuning superconductivity in twisted bilayer graphene *Science* **363** 1059–64
[12] Balents L, Dean C R, Efetov D K and Young A F 2020 Superconductivity and strong correlations in moiré flat bands *Nat. Phys.* **16** 725–33
[13] Saito Y, Ge J, Watanabe K, Taniguchi T and Young A F 2020 Independent superconductors and correlated insulators in twisted bilayer graphene *Nat. Phys.* **16** 926–30
[14] Jorio A and Cançado L G 2013 Raman spectroscopy of twisted bilayer graphene *Solid State Commun.* **175–176** 3–12
[15] Eliel G S N *et al* 2018 Intralayer and interlayer electron-phonon interactions in twisted graphene heterostructures *Nat. Commun.* **9** 1221

[16] Angeli M, Tosatti E and Fabrizio M 2019 Valley Jahn-Teller effect in twisted bilayer graphene *Phys. Rev.* X **9** 041010
[17] Wu F, MacDonald A H and Martin I 2018 Theory of phonon-mediated superconductivity in twisted bilayer graphene *Phys. Rev. Lett.* **121** 257001
[18] Wu F, Hwang E and Das Sarma S 2019 Phonon-induced giant linear-in-T resistivity in magic angle twisted bilayer graphene: ordinary strangeness and exotic superconductivity *Phys. Rev.* B **99** 165112
[19] Lian B, Wang Z and Bernevig B A 2019 Twisted bilayer graphene: a phonon-driven superconductor *Phys. Rev. Lett.* **122** 257002
[20] Ferrari A C and Basko D M 2013 Raman spectroscopy as a versatile tool for studying the properties of graphene *Nat. Nanotechnol.* **8** 235–46
[21] Malard L M, Pimenta M A, Dresselhaus G and Dresselhaus M S 2009 Raman spectroscopy in graphene *Phys. Rep.* **473** 51–87
[22] Saito R, Hofmann M, Dresselhaus G, Jorio A and Dresselhaus M S 2011 Raman spectroscopy of graphene and carbon nanotubes *Adv. Phys.* **60** 413–550
[23] Jorio A, Saito R, Dresselhaus G and Dresselhaus M S 2011 *Raman Spectroscopy in Graphene Related Systems* (Weinheim: Wiley-VCH Verlag GmbH & Co. KGaA) (https://doi.org/10.1002/9783527632695)
[24] Ni Z, Liu L, Wang Y, Zheng Z, Li L J, Yu T and Shen Z 2009 G -band Raman double resonance in twisted bilayer graphene: evidence of band splitting and folding *Phys. Rev.* B **80** 1–5
[25] Carozo V, Almeida C M, Ferreira E H M, Cançado L G, Achete C A and Jorio A 2011 Raman signature of graphene superlattices *Nano Lett.* **11** 4527–34
[26] Eliel G S N, Ribeiro H B, Sato K, Saito R, Lu C C, Chiu P W, Fantini C, Righi A and Pimenta M A 2017 Raman excitation profile of the G-band enhancement in twisted bilayer graphene *Braz. J. Phys.* **47** 589–93
[27] Ribeiro H B, Sato K, Eliel G S N, de Souza E A T, Lu C-C, Chiu P-W, Saito R and Pimenta M A 2015 Origin of van Hove singularities in twisted bilayer graphene *Carbon* **90** 138–45
[28] Kim K, Coh S, Tan L Z, Regan W, Yuk J M, Chatterjee E, Crommie M F, Cohen M L, Louie S G and Zettl A 2012 Raman spectroscopy study of rotated double-layer graphene: misorientation-angle dependence of electronic structure *Phys. Rev. Lett.* **108** 246103
[29] Sato K, Saito R, Cong C, Yu T and Dresselhaus M S 2012 Zone folding effect in Raman G-band intensity of twisted bilayer graphene *Phys. Rev.* B **86** 125414
[30] Havener R W, Zhuang H, Brown L, Hennig R G and Park J 2012 Angle-resolved Raman imaging of interlayer rotations and interactions in twisted bilayer graphene *Nano Lett.* **12** 3162–7
[31] Kalbac M, Frank O, Kong J, Sanchez-Yamagishi J, Watanabe K, Taniguchi T, Jarillo-Herrero P and Dresselhaus M S 2012 Large variations of the Raman signal in the spectra of twisted bilayer graphene on a BN substrate *J. Phys. Chem. Lett.* **3** 796–9
[32] Campos-Delgado J, Cançado L G, Achete C A, Jorio A and Raskin J P 2013 Raman scattering study of the phonon dispersion in twisted bilayer graphene *Nano Res.* **6** 269–74
[33] Carozo V *et al* 2013 Resonance effects on the Raman spectra of graphene superlattices *Phys. Rev.* B **88** 085401
[34] Righi A, Costa S D, Chacham H, Fantini C, Venezuela P, Magnuson C, Colombo L, Bacsa W S, Ruoff R S and Pimenta M A 2011 Graphene Moiré patterns observed by umklapp double-resonance Raman scattering *Phys. Rev.* B **84** 241409
[35] He R, Chung T F, Delaney C, Keiser C, Jauregui L A, Shand P M, Chancey C C, Wang Y, Bao J and Chen Y P 2013 Observation of low energy Raman modes in twisted bilayer graphene *Nano Lett.* **13** 3594–601
[36] Gadelha A C *et al* 2021 Localization of lattice dynamics in low-angle twisted bilayer graphene *Nature* **590** 405–9
[37] Hung Nguyen V, Paszko D, Lamparski M, Van Troeye B, Meunier V and Charlier J-C 2021 Electronic localization in small-angle twisted bilayer graphene *2D Mater.* **8** 035046
[38] Li G, Luican A, Lopes Dos Santos J M B, Castro Neto A H, Reina A, Kong J and Andrei E Y 2010 Observation of Van Hove singularities in twisted graphene layers *Nat. Phys.* **6** 109–13
[39] Novoselov K S, Geim A K, Morozov S V, Jiang D, Zhang Y, Dubonos S V, Grigorieva I V and Firsov A A 2004 Electric field in atomically thin carbon films *Science* **306** 666–9
[40] Kim K *et al* 2016 Van der Waals heterostructures with high accuracy rotational alignment *Nano Lett.* **16** 1989–95
[41] Gadelha A C *et al* 2021 Twisted bilayer graphene: a versatile fabrication method and the detection of variable nanometric strain caused by twist-angle disorder *ACS Appl. Nano Mater.* **4** 1858–66
[42] Dean C R *et al* 2010 Boron nitride substrates for high-quality graphene electronics *Nat. Nanotechnol.* **5** 722–6
[43] Ohlberg D A A *et al* 2021 The limits of near field immersion microwave microscopy evaluated by imaging bilayer graphene moiré patterns *Nat. Commun.* **12** 2980
[44] Beyer H, Müller M and Schimmel T 1999 Monolayers of graphite rotated by a defined angle: hexagonal superstructures by STM *Appl. Phys.* A **68** 163–6
[45] Ferrari A C *et al* 2006 Raman spectrum of graphene and graphene layers *Phys. Rev. Lett.* **97** 187401
[46] Saito R, Jorio A, Souza Filho A G, Dresselhaus G, Dresselhaus M S and Pimenta M A 2001 Probing phonon dispersion relations of graphite by double resonance Raman scattering *Phys. Rev. Lett.* **88** 027401
[47] Lee J E, Ahn G, Shim J, Lee Y S and Ryu S 2012 Optical separation of mechanical strain from charge doping in graphene *Nat. Commun.* **3** 1024
[48] Cançado L G, Pimenta M A, Saito R, Jorio A, Ladeira L O, Grueneis A, Souza-Filho A G, Dresselhaus G, Dresselhaus M S and Dresselhaus M S 2002 Stokes and anti-Stokes double resonance Raman scattering in two-dimensional graphite *Phys. Rev.* B **66** 354151–5
[49] Souza Filho A G *et al* 2002 Anomalous two-peak G′-band Raman effect in one isolated single-wall carbon nanotube *Phys. Rev.* B **65** 085417
[50] Maultzsch J, Reich S and Thomsen C 2004 Double-resonant Raman scattering in graphite: interference effects, selection rules, and phonon dispersion *Phys. Rev.* B **70** 155403
[51] Barros E B, Souza Filho A G, Son H and Dresselhaus M S 2007 G′ band Raman lineshape analysis in graphitic foams *Vib. Spectrosc.* **45** 122–7
[52] Mohr M, Maultzsch J and Thomsen C 2010 Splitting of the Raman 2D band of graphene subjected to strain *Phys. Rev.* B **82** 201409
[53] Venezuela P, Lazzeri M and Mauri F 2011 Theory of double-resonant Raman spectra in graphene: intensity and line shape of defect-induced and two-phonon bands *Phys. Rev.* B **84** 1–25
[54] Temme N M 2010 *NIST Digital Library of Mathematical Functions, 1.1.4* (https://dlmf.nist.gov/7.21) (Accessed 21 January 2022)
[55] Mafra D L, Malard L M, Doorn S K, Htoon H, Nilsson J, Castro Neto A H and Pimenta M A 2009 Observation of the Kohn anomaly near the K point of bilayer graphene *Phys. Rev.* B **80** 241414
[56] Wertheim G K, Butler M A, West K W and Buchanan D N E 1974 Determination of the Gaussian and Lorentzian content of experimental line shapes *Rev. Sci. Instrum.* **45** 1369–71
[57] Alstrom T S, Schmidt M N, Rindzevicius T, Boisen A and Larsen J 2017 A pseudo-Voigt component model for high-resolution recovery of constituent spectra in Raman spectroscopy *IEEE Int. Conf. Acoust. Speech Signal Process.—Proc. (ICASSP)* pp 2317–21
[58] Yoo H *et al* 2019 Atomic and electronic reconstruction at the van der Waals interface in twisted bilayer graphene *Nat. Mater.* **18** 448–53

[59] Gargiulo F and Yazyev O V 2017 Structural and electronic transformation in low-angle twisted bilayer graphene *2D Mater.* **5** 015019
[60] Alden J S, Tsen A W, Huang P Y, Hovden R, Brown L, Park J, Muller D A and McEuen P L 2013 Strain solitons and topological defects in bilayer graphene *Proc. Natl Acad. Sci.* **110** 11256–60
[61] Jiang L *et al* 2016 Soliton-dependent plasmon reflection at bilayer graphene domain walls *Nat. Mater.* **15** 840–4
[62] Hasdeo E H, Nugraha A R T, Dresselhaus M S and Saito R 2016 Fermi energy dependence of first- and second-order Raman spectra in graphene: Kohn anomaly and quantum interference effect *Phys. Rev.* B **94** 075104
[63] Piscanec S, Lazzeri M, Mauri F, Ferrari A C and Robertson J 2004 Kohn anomalies and electron-phonon interactions in graphite *Phys. Rev. Lett.* **93** 185503
[64] Pisana S, Lazzeri M, Casiraghi C, Novoselov K S, Geim A K, Ferrari A C and Mauri F 2007 Breakdown of the adiabatic Born-Oppenheimer approximation in graphene *Nat. Mater.* **6** 198–201
[65] Das A, Chakraborty B, Piscanec S, Pisana S, Sood A K and Ferrari A C 2009 Phonon renormalization in doped bilayer graphene *Phys. Rev.* B **79** 155417
[66] Hung Nguyen V, Paszko D, Lamparski M, Van Troeye B, Meunier V and Charlier J-C 2021 Electronic localization in small-angle twisted bilayer graphene (arXiv:2102.05376)
[67] Uri A *et al* 2020 Mapping the twist-angle disorder and Landau levels in magic-angle graphene *Nature* **581** 47–52